Detection of Multilayer Cirrus Cloud Systems Using AVHRR Data: Verification Based on FIRE II IFO Composite Measurements

S. C. OU AND K. N. LIOU

Department of Meteorology/CARSS, University of Utah, Salt Lake City, Utah

B. A. BAUM

Atmospheric Sciences Division, NASA/Langley Research Center, Hampton, Virginia

(Manuscript received 4 April 1995, in final form 8 August 1995)

ABSTRACT

A numerical scheme has been developed to identify multilayer cirrus cloud systems using Advanced Very High Resolution Radiometer (AVHRR) data. It is based on the physical properties of the AVHRR channels 1–2 reflectance ratios, the brightness temperature differences between channels 4 and 5, and the channel 4 brightness temperatures. In this scheme, clear pixels are first separated from cloudy pixels, which are then classified into three types: cirrus, cirrus/low cloud, and low clouds. The authors have applied this scheme to the satellite data collected over the FIRE II IFO [First ISCCP (International Satellite Cloud Climatology Project) Regional Experiment II intensive field observation] area during nine overpasses within seven observation dates. Determination of the threshold values used in the detection scheme are based on statistical analyses of these satellite data. The authors have validated the detection results against the cloudy conditions inferred from the collocated and coincident ground-based lidar and radar images, balloonborne replicator data, and National Center for Atmospheric Research CLASS (Cross-chain Loran Atmospheric Sounding System) humidity soundings on a case-by-case basis. In every case, the satellite detection results are consistent with the cloudy conditions inferred from these independent and complementary measurements. The present scheme is well suited for the detection of midlatitude, multilayer cirrus cloud systems and tropical anvils.

1. Introduction

Cirrus clouds have been recognized as playing a key role in the global radiative energy balance and climate change (Liou 1986). Information on cirrus cloud parameters is, therefore, critically important to the development of cirrus cloud formation models, the upgrade of real-time global cloud analyses, and the computation of atmospheric and surface radiative parameters in climate and general circulation models.

We have developed a novel and comprehensive remote sensing algorithm for the retrieval of cirrus cloud temperature, optical depth, and mean effective ice crystal size using Advanced Very High Resolution Radiometer (AVHRR) data (Ou et al. 1993; Rao et al. 1995). Validation of this cirrus remote sensing program has been carried out using the local daytime satellite data collected during the FIRE I and FIRE II IFOs [First ISCCP (International Satellite Cloud Climatology Project) Regional Experiments I and II intensive field observations] (Rao et al. 1995; Ou et al. 1995).

Corresponding author address: Dr. S. C. Ou, Department of Meteorology/CARSS, University of Utah, 821 William C. Browning Building, Salt Lake City, UT 84112.

A very important procedure in determining cirrus cloud parameters is the detection of the sky condition within the field of view of satellite radiometers. Previously, our detection scheme has been developed primarily for application to single-layer cirrus clouds. Many satellite cloud detection methods have also been developed based on the assumption that clouds exist in single-layer form (e.g., Minnis and Harrison 1984; Arking and Childs 1985; Chou et al. 1986; d'Entremont 1986; Saunders and Kriebel 1988). In particular, a visible-threshold approach has been developed by Minnis et al. (1990) to filter out probable multilayer cloud pixels in their cirrus cloud retrieval scheme.

Surface observations show that multilayer clouds frequently occur in frontal areas where cirrus clouds overlie boundary layer convective clouds or stratus clouds (Hahn et al. 1982, 1984; Tian and Curry 1989). Baum et al. (1994) have used data from coincident and collocated High-Resolution Infrared Radiation Sounder (HIRS) 15-μm sounder channels and AVHRR thermal infrared channels to detect multilayer clouds. In their approach, the observed relationship between the brightness temperature differences and channel 4 brightness temperatures is established by utilizing detailed radiative transfer calculations based on prescribed cloud microphysics models. This scheme has

been applied for the detection of multilayer cirrus clouds occurring over the FIRE II IFO region, and verification has been made against CO_2 lidar and 94-GHz radar measurements (Baum et al. 1995).

In this paper, we describe a numerical scheme for detecting multilayer cirrus pixels using data from AVHRR channels 1 (0.63 μm), 2 (0.86 μm), 4 (10.9 μm), and 5 (12.0 μm). The scheme is based on the physical properties of the channels 2–1 reflectance ratios, brightness temperature differences between channels 4 and 5, and channel 4 brightness temperatures over clear, cirrus, and cirrus/low cloud regions. In section 2, the detection methodology is presented. In section 3, we discuss application of the detection scheme to the satellite data collected over the FIRE II IFO region for several representative dates. Validation of the detection results is performed using available ground-based lidar and radar measurements, balloonborne replicator data, and humidity profiles determined from National Center for Atmospheric Research (NCAR) CLASS (Cross-chain Loran Atmospheric Sounding System) soundings. Finally, conclusions are given in section 4.

2. The detection of multilayer cirrus pixels

During daytime, with the availability of visible channel data, differentiation between clear and cloudy conditions over various types of surfaces can be made using the following criteria.

First, we can utilize the AVHRR channel 1 reflectance r_1. Clouds generally reflect more visible light than most types of land and water surfaces, except snow and ice or highly reflecting desert. For this reason, we can set a threshold value r_{1c} such that $r_1 < r_{1c}$ is a necessary condition for the presence of clear pixels. This threshold value can be determined empirically by identifying the peaks corresponding to the cloudy and clear conditions in the r_1 histogram.

Second, under certain cloudy conditions, the reflectances for channels 1 and 2 are of the same order of magnitude. However, over land and vegetation surfaces, $r_1 < r_2$, whereas over water, $r_1 > r_2$. We can define a ratio $Q = r_2/r_1$ and use two thresholds Q_1 and Q_2 to identify cloudy and clear pixels over land and water surfaces, respectively. A clear water or land peak can be determined from the histogram of Q. The threshold Q_1 is then defined as the value less than the clear land peak by a standard deviation. If there is no well-defined peak, a uniform value is set for Q_1. The threshold Q_2 is defined as the value greater than the clear water peak by a standard deviation. Pixels with $Q > Q_1$ or $Q < Q_2$ are identified as clear.

Third, we can also use the IR brightness temperature to identify clear and cloudy conditions. The channel 4 brightness temperature T_4 for a clear pixel must be higher than that for a cloudy pixel. Thus, we may set a threshold temperature T_{4cr} such that $T_4 > T_{4cr}$ represents clear conditions; T_{4cr} is empirically set as $\bar{T}_4 - \delta$, where $\bar{T}_4$ is an estimated mean clear brightness temperature and δ is an adjustment factor.

Fourth, over clear regions, because of the behavior of Planck functions and atmospheric transmissions for channels 4 and 5, one finds that the brightness temperature difference (BTD45) is less than a prescribed value $BTD45_{cr}$, which is about 2.5 K (Inoue 1987).

If a pixel satisfies the preceding four criteria, it can be identified as clear. In this manner, clear and cloudy conditions can be differentiated by numerical testing. These four criteria, which use visible radiances and IR brightness temperatures, are necessary and sufficient to identify the clear condition. For example, criterion 4 also applies for thermally black clouds. However, these clouds are usually optically thick, allowing criterion 1 to discriminate them from clear cases. In the case of thin cirrus clouds, criterion 4 can be used to separate them from clear cases. The clear detection scheme is schematically shown in the left column of Fig. 1.

After all the cloudy pixels are identified, they are further categorized into three classes: cirrus, cirrus/low cloud, and low cloud. Here, "cirrus" may be cirrus (Ci), cirrostratus (Cs), or cirrocumulus (Cc), and "low cloud" may be cumulus (Cu), stratus (St), stratocumulus (Sc), altostratus (As), or altocumulus (Ac). First, we use the channel 4 brightness temperatures to detect optically thick cirrus clouds. We can identify pixels with T_4 less than a prescribed tempera-

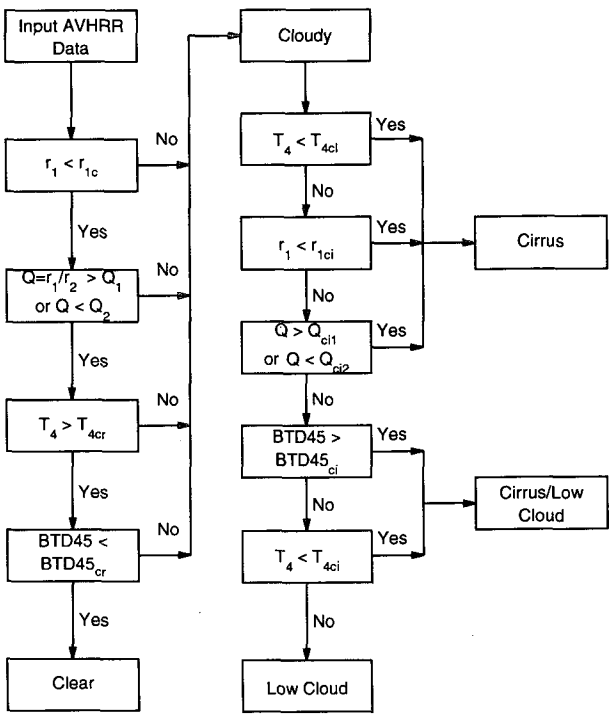

FIG. 1. Flowchart of the detection scheme for the identification of clear, cirrus, low, and cirrus/low-cloud conditions.

ture T_{4c1} as thick cirrus, where T_{4c1} is about 233 K. The temperatures of cirrus clouds are always colder than the observed T_4 because of their semitransparent nature. According to laboratory data on the freezing of pure water, 233 K is the spontaneous freezing point for droplets smaller than 5 μm (Rogers and Yau 1989). Thus, if a cloud is located in temperatures colder than 233 K, this cloud is most likely composed of ice crystals. Moreover, if T_4 is colder than 233 K, the cloud must be optically thick. This is because for thin cirrus a significant amount of emission from below-cloud sources (low-level cloud or ground surface) at a much higher temperature will be transmitted through the cloud with a brightness temperature well above 233 K, based on observed data. Lower cloud layers may exist beneath the optically thick cirrus clouds. However, since radiances detected by satellite are mainly from thick cirrus, it is difficult to determine the presence or absence of these lower cloud layers.

Second, the visible channel reflectances for low clouds are generally larger than those for cirrus clouds, because the former are composed of water droplets with relatively small sizes and high number concentrations and are generally optically thicker than the latter (Liou 1992, Table 4.2). For this reason, a visible channel threshold r_{1ci} can be established to filter out those pixels that contain low clouds. Minnis et al. (1990) suggested that this threshold value is about 0.2. Thus, pixels that have channel 1 reflectances smaller than r_{1ci} can then be identified as cirrus. Note, however, that certain optically thick cirrus clouds can produce high reflectances and may not be distinguished solely by this visible threshold test. In addition, some midlevel clouds can have reflectances less than 0.2, but their occurrences are rare (Rossow and Lacis 1990, Fig. 10).

Third, we also use the Q ratio to classify cirrus clouds. This part of the detection scheme is based on the following physical principle. The peak on the histogram of the Q ratio for cloudy pixels varies between 0.8 and 1.1. The Q ratio becomes larger over higher clouds, where channel 1 reflected radiances are absorbed by stratospheric ozone in the Chappuis band and the effects of below-cloud weak absorption by tropospheric water vapor in the 0.94-μm region are shielded by cirrus clouds. When clouds are lower, the reduction of channel 2 reflected radiances due to absorption by tropospheric water vapor becomes significant, leading to the decrease of the Q ratio (Saunders and Kriebel 1988). Thus, the Q ratio for low clouds is usually smaller than that for cirrus clouds. In addition, the Q ratio for cirrus over land is larger than that for cirrus over low clouds, because the channel 1 reflectance is less than the channel 2 reflectance for land surface, although they are about the same in the low-cloud case. However, the Q ratio for cirrus over water is smaller than that for cirrus over low clouds, because the channel 1 reflectance is larger than the channel 2 reflectance for water surface. Based on the above physical reasonings, threshold values Q_{ci1} and Q_{ci2} are established such that the pixels contain cirrus if $Q > Q_{ci1}$ over land or $Q < Q_{ci2}$ over water. Otherwise, they may be associated with either low cloud or cirrus/low cloud.

The preceding three criteria are used to separate single-layer cirrus from cirrus/low-cloud and low-cloud conditions. We use BTD45 to differentiate cirrus/low from low cloud. For nonblack cirrus clouds, the channel 4 brightness temperature is larger than that of channel 5. The reason for this behavior is as follows. The emissivity of cirrus for channel 4 is usually less than that for channel 5, leading to more transmission of warmer radiation from below and, consequently, to larger brightness temperature. However, for low-level clouds that are thermally black, the channel 4 brightness temperature is about the same as that of channel 5. Thus, we can establish a threshold $BTD45_{ci}$ to differentiate the presence of nonblack cirrus clouds with low clouds below from black low clouds. Moreover, we use $T_4 > T_{4ci}$ to discriminate cirrus/low cloud from low cloud, where T_{4ci} is a threshold temperature set at 253 K. Above this temperature, the cloud is most likely composed only of water droplets (Matveev 1984). The cloud detection scheme is illustrated schematically in the middle and right columns of Fig. 1.

3. Application of the detection scheme to the FIRE II IFO data

a. Data sources

The FIRE II IFO was carried out near Coffeyville, Kansas (37.10°N, 95.57°W), during November and December 1991. One of the objectives of this field experiment was to quantify the capabilities and limitations of methods for retrieving physical and optical properties of cirrus clouds from satellite observations. During the latter part of November and the first part of December, a total of 11 cirrus days was observed. We have reviewed the available satellite data, lidar, 94-GHz radar, and sounding measurements for these dates. Many of these dates were associated with multilayer cloudy conditions.

For the detection of cirrus cloud pixels, we use high-resolution HRPT (High Resolution Picture Transmission) AVHRR data from *NOAA-11* and *NOAA-12* polar-orbiting satellites. The daytime overpasses for *NOAA-11* and *NOAA-12* near Coffeyville are around 2000 and 1400 UTC, respectively. There are 2048 pixels in an HRPT scan line. The spatial resolution of each pixel near the nadir of the satellite is 1.1 km × 1.1 km. The NIR and IR radiances were calculated from the raw counts provided in the *NOAA-1b* data stream using the nominal calibration (Kidwell 1991) and from the nonlinearity corrections described by Weinreb et al. (1990). The visible channel radiances were calculated using the instrument degradation correction function provided by Whitlock et al. (1994).

To validate the detection results, we have acquired ground-based lidar backscatter data and radar reflectivity measurements obtained over Coffeyville and Parsons, Kansas, during FIRE II IFO. The Pennsylvania State University (PSU) radar (Clothiaux et al. 1995) located at Coffeyville operated at 94 GHz (= 3.19 mm) in the backscatter mode. The PSU radar was a two-dish system that was pointed in the vertical during data collection periods. The radar had a 0.25° beamwidth and a minimum vertical resolution of 7.5 m. Variable resolution data were obtained typically to 30-m resolution.

The Doppler lidar operated by the National Oceanic and Atmospheric Administration (NOAA) Environmental Technology Laboratory (ETL) was also located at Coffeyville (Uttal and Intrieri 1993). The lidar was a mobile, pulsed, coherent CO_2 laser radar system (Post and Cupp 1990). During FIRE II IFO, the lidar operated at a wavelength of 10.6 μm, which measured the radial wind velocities and backscattered signal intensity with ranges as large as 30 km. The lidar was pointed vertically during most of the mission. Observations were recorded at a rate of 8 Hz, and 15-m range gates were averaged to 75 m in postprocessing. The lidar was periodically moved back and forth a few degrees from the vertical to check whether specular reflections were occurring.

Additional lidar data were provided by the National Aeronautics and Space Administration (NASA) Langley Research Center (LaRc) researchers who were stationed at a field site near Parsons (Alvarez 1994). The lidar deployed at this site was composed of a frequency-doubled Nd:YAG (neodymium-doped:yttrium aluminum garnet) laser with an 8″ Cassegrain telescope and a depolarization-sensitive receiver system. The system had a wavelength of 532 nm, and the vertical resolution of the data was 30 m. This lidar was usually pointed vertically, although it was periodically tilted 6° off the vertical to detect horizontally oriented ice crystals. Each lidar record was composed of 150 hardware-averaged lidar returns, yielding a temporal resolution of 15 s.

Uttal and Intrieri (1993) and Baum et al. (1995) showed that lidars and radars operating at different wavelengths could detect cloud boundaries located at different heights. In general, an instrument senses clouds that are composed of particles whose sizes are of the same order or larger than the instrument's wavelength. Particles much smaller than the wavelength tend to be transparent because of their very small extinction efficiency. The optical properties of ice or water, with respect to the incident wavelength, can also play an important role.

High vertical resolution sonde data were collected from the NCAR CLASS from Coffeyville during FIRE II IFO. The sonde temperature and relative humidity profiles were provided at approximately 400 pressure levels. These profiles were used as an aid for the identification of both stratus and cirrus cloud altitudes. Moreover, balloonborne formvar ice crystal replicators were launched with the NCAR CLASS during FIRE II IFO to measure the "vertical profiles" (in a Lagrangian sense) of cirrus microphysical properties, with emphasis on the detection of small ice particles. Replicator launches were timed to coincide with satellite overpasses and with the time periods when ground-based remote sensors and aircraft were operating. The replicator data were also used to determine the cirrus cloud boundaries.

Based on the availability of verification datasets, we have selected seven representative dates for our study, including clear, cirrus, and cirrus/low-cloud conditions. The weather synopsis for each date around Coffeyville area is given in the following.

- 6 December

Morning temperatures were above freezing. Cirrus clouds moved over the region in the early morning at altitudes from 7 to 9 km. Some low-level stratus came over the area from the south during the morning, but by noon the clouds had largely disappeared, including the cirrus.

- 5 December

The sky was clear at sunrise and not very cold. A rapid influx of light cirrus (spissatus) was observed from the west during the morning. Coverage and density of cirrus increased throughout the day. Aircraft- and ground-based sensors estimated cloud bases in the 10-km range, with tops extending to about 13 km. During late afternoon, multilayer features covered the sky, with all stations in Kansas reporting high-level clouds. No low- or middle-level clouds passed over Coffeyville, but some low clouds were visible in the distant southern sky during the afternoon.

- 26 November

Clear and cold conditions existed over southeastern Kansas at sunrise. Around noon, cirrus spissatus began to spread over the area. By 2000 UTC, a broken cirrus layer was evident from 8.5 to 9.5 km, which grew increasingly thicker. Lidars also reported a midlevel cloud layer (~6.5 km) at that time. Surface reports indicated that clouds were located at multiple levels to the north and west of Coffeyville. By late afternoon, multilayered cloud conditions, including a low-level cloud deck, prevailed with continued strong southerly winds.

- 22 November

This was a transition date for weather in southeastern Kansas. Following the late-night clearing event at about 0200 LT, patchy cirrus increased to total overcast during the morning hours. However, middle- and low-level clouds also increased dramatically. By noon, the sky was completely overcast with low- and middle-level clouds.

- 29 November

This was a very cloudy day with a fairly dense low-level stratus overcast that was sometimes broken. There were occasional glimpses of the overlying cirrus shield

TABLE 1. Statistics of various parameters used in the cloud detection scheme for different FIRE II IFO dates. Except for the 11/27a case, all other cases are over a 1.0° × 1.0° area around Coffeyville. The 11/27a case is over a 1.0° × 1.0° area around 38.5°N, 96.5°W. The definition of the symbols is as follows—r_1: channel 1 reflectance; Q: ratio of channel 2 to channel 1 radiances; BTD45: brightness temperature difference between channel 4 and channel 5; T_4: channel 4 brightness temperature; a: *NOAA-12* overpass (~1400 UTC); b: *NOAA-11* overpass (~2100 UTC); mean: average value of a particular parameter within the domain; std dev: standard deviation of the parameter.

Date	Number of pixels	r_1 (%)		Q		BTD45 (K)		T_4 (K)	
		Mean	Std dev	Mean	Std dev	Mean	Std dev	Mean	Std dev
12/6b	8484	13.7	4.2	1.17	0.079	1.02	0.21	287	1.2
12/5b	7226	24.7	5.3	1.09	0.032	2.96	0.61	260	7.6
11/26b	7650	39.7	10.4	1.02	0.030	2.01	0.70	249	11.7
11/22a	9970	45.8	15.4	0.90	0.031	0.45	0.64	245	6.8
11/29a	5781	47.1	10.5	0.89	0.042	0.88	0.70	243	8.5
11/28a	7904	31.4	8.5	0.90	0.044	2.21	0.53	269	6.5
11/28b	8954	29.2	10.7	1.03	0.034	2.21	0.51	272	10.8
11/27a	5200	44.5	8.2	0.91	0.019	0.80	0.90	246	4.5
11/27b	8183	65.0	9.5	0.93	0.018	3.78	1.12	256	9.6

and occasional spits of drizzle. Strong thunderstorms moved through the Coffeyville area around 1400 LT followed by a second line just before sunset. A tornado was reported in the Tulsa, Oklahoma, area and later near Springfield, Missouri. Winds turned westerly, and the skies cleared after passage of the prefrontal thunderstorm system.

- 28 November

This date was warm and windy. Early morning showers produced mostly cloudy skies with low-level broken clouds and scattered to broken cirrus clouds.

- 27 November

An overcast of low clouds remained over the Coffeyville area all day. The southerly flow at the low levels had brought moisture and clouds from Texas near the end of the previous day. A uniform deck of "ridge crest" cirrus covered southeastern Kansas during most of the day.

b. *Determination of threshold values based on FIRE II IFO satellite data*

Table 1 shows the statistics of various parameters used for the determination of threshold values in the cloud detection scheme. The first column is the date in the form of month/date-satellite code. We have selected nine satellite overpasses within the seven dates. Except for the case of 27 November associated with *NOAA-12,* statistical analyses of the AVHRR channel data were performed over a 1.0° × 1.0° area around Coffeyville. Analysis of the 27 November case was performed over a 1.0° × 1.0° area northwest of Coffeyville, where a significant presence of clouds was noted. The size of the analysis domain guarantees a large enough statistical sample of satellite data. Based on the above weather synopses, we were able to determine the general cloudy situation around Coffeyville at the time of satellite overpass. A clear case occurred on 6 December. Both 5 December and 26 November were cases involving single-layer cirrus (Ou et al. 1995). The remaining cases were largely associated with multilayer clouds. In particular, 22 November involved mixed-phase cloud, in which the ice cloud layer overlaid the water cloud layer in a contiguous manner as indicated by the balloonborne replicator measurements.[1] The number of pixels analyzed in each case ranges between 5000 and 10 000.

We have computed four parameters for each pixel: r_1, Q, BTD45, and T_4. All these parameters are used in the cloud detection scheme. For each parameter, we construct a one-dimensional histogram using data of all pixels within the domain and compute the mean value of that parameter and its standard deviation. Based on the values listed in Table 1, different characteristics for these parameters are shown for different cloudy conditions. These statistics reveal that distinctive thresholds can be set for each cloud/clear test. The mean r_1 for the clear domain is the smallest but it is the largest for multilayer cloudy domains. The presence of low-level stratiform water clouds always increases the mean r_1 significantly, as evidenced by the mixed-phase and multilayer cloudy cases. The standard deviation of r_1 for the clear case is only 4.2%, revealing that the atmospheric and surface conditions were relatively uniform. A similar conclusion can be made for the 5 December cirrus case. The rest of the cloudy cases all show r_1 standard deviations larger than 8%, indicating that the clouds are highly inhomogeneous.

The behavior of the mean Q ratio is the most interesting. The maximum mean Q ratio (1.17) occurs for the only clear case. Both single-layer cirrus cases show mean Q-ratio values slightly larger than 1. All the rest of the cloudy cases reveal mean Q ratios less than 1

[1] On 22 November, the NCAR CLASS sounding was launched from Coffeyville at 1416 UTC. Navigational data show that by the time the balloon reached cloud base (4.6 km) and top (8.8 km) it was located at 37.19°N, 95.53°W and at 37.26°N, 95.38°W, respectively. These coordinates are well within the 1.0° × 1.0° satellite data analysis domain.

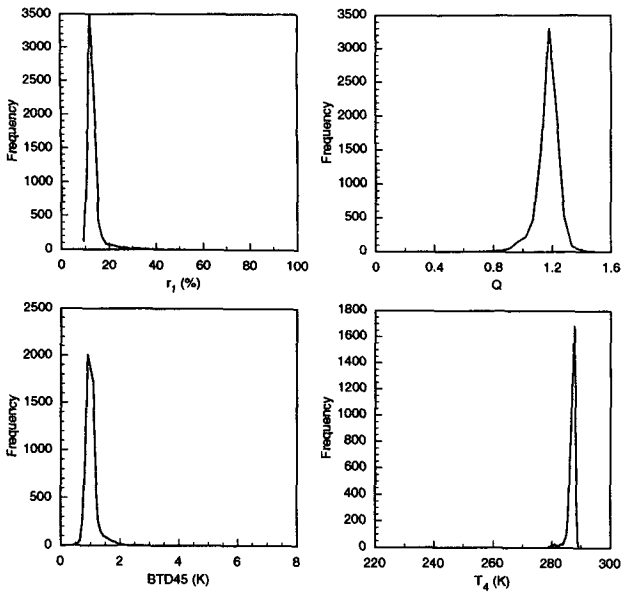

FIG. 2. Histograms of channel 1 reflectance r_1, channels 2–1 reflectance ratio Q, channels 4–5 brightness temperature difference BTD45, and channel 4 brightness temperature T_4 for the case of 2000 UTC 6 December 1991.

except for the 2100 UTC 28 November case, in which $Q = 1.03$ due to the presence of some broken low clouds within the domain. Thus, it is possible to use the Q ratio to separate single-layer cirrus from cirrus/low clouds in overcast conditions. The standard deviations of the Q ratio for cloudy cases are all less than 0.05. Saunders and Kriebel (1989) proposed to use the

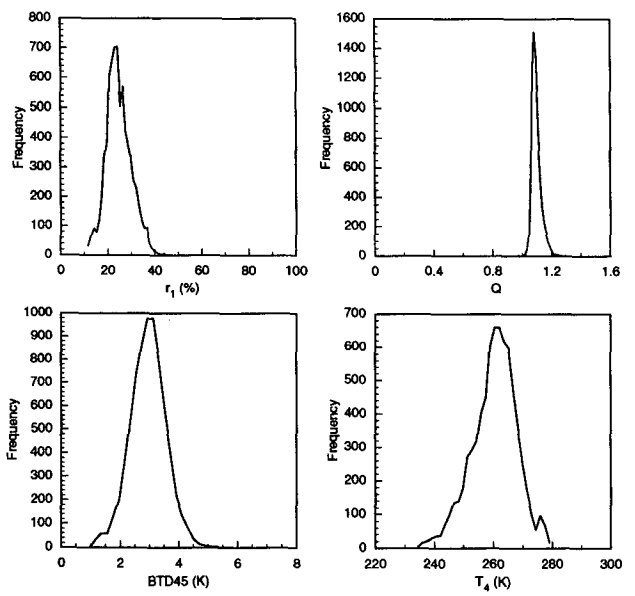

FIG. 3. Same as Fig. 2 except for the case of 2100 UTC 5 December 1991.

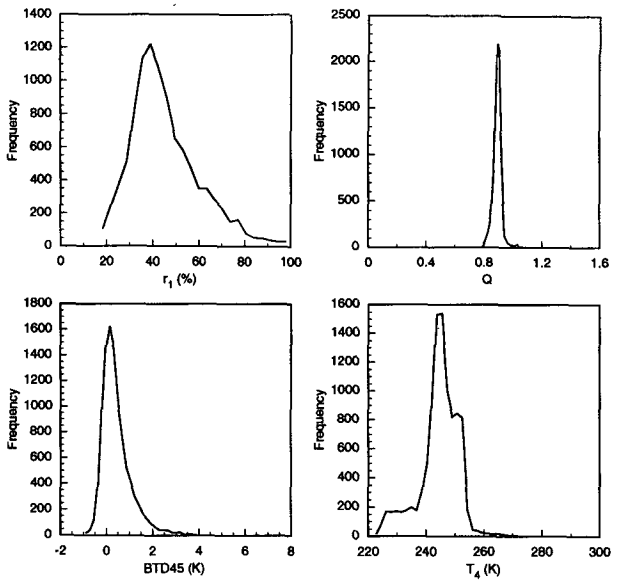

FIG. 4. Same as Fig. 2 except for the case of 1400 UTC 22 November 1991.

difference between Q ratios associated with individual pixels and the mode value within a domain to detect partially cloudy pixels. They assumed that if this difference is larger than 0.05 the pixel is partially cloudy. Based on this criterion, the pixels in the present cloudy cases are mostly overcast, because the standard deviations for the Q ratios are all smaller than 0.05. It follows that most of the pixels are suitable for the retrieval of cirrus cloud microphysical and optical properties using the method developed by Ou et al. (1993).

The behavior of BTD45 also shows a specific pattern. The mean BTD45 for the two cirrus cases are both larger than 2 K. The mean BTD45 for the mixed-phase cloudy case is 0.45 K, signifying that the cloud system approaches blackbody. For the rest of the cloudy cases, the mean values of BTD45 range between 0.80 and 3.78 K. Finally, the mean values of T_4 for all cloudy cases are smaller than 273 K.

Histograms of r_1, Q, BTD45, and T_4 constructed from satellite data for three representative cases (12/6b, 12/5b, and 11/22a) are shown in Figs. 2–4. In the

TABLE 2. Threshold values used in the clear/cloud detection scheme.

Clear detection		Cloudy detection	
Threshold	Value	Threshold	Value
r_{1c}	0.18	r_{1ci}	0.20
Q_1	1.10	Q_{ci1}	1.00
T_{4cr}	280.0 K	T_{4ci}	253.0 K
$BTD45_{cr}$	2.5 K	$BTD45_{ci}$	0.5 K
		T_{4cl}	233.0 K

present study, all histograms show a distinctive frequency peak for each parameter. The narrowness of the distribution shape indicates the uniformity of the clear/cloudy situation in each case. Thus, based on all histograms and the associated mean values and standard deviations, we can determine the threshold values for the detection scheme. Threshold values for various tests in the cloud detection scheme are listed in Table 2. Only r_{1c}, Q_1, and T_{4cr} need to be recomputed for different geographical regions and time periods. The rest of the threshold values are derived based on physical principles. Hence, they can be applied to all situations.

c. *Application of the cloud detection scheme to AVHRR data*

We compile the percentage of pixels classified as clear, cirrus, cirrus/low, and low cloud by the detection scheme over the Coffeyville area for the preceding observation dates (Table 3). Except for the 12/6b and 11/28b cases, all others are identified by the detection scheme as being 100% cloud coverage. The 12/6b case is identified as mostly clear sky over Coffeyville with cirrus over the southeastern corner of the domain (see Fig. 5a). The 11/28b case contains small, clear holes within the cirrus deck. Results of both cases agree with the weather synopses. For the 12/5b and 11/26b cases, 99.9% and 84.5% of pixels are identified as cirrus. According to weather synopses, the Coffeyville area was covered with single-layer cirrus on both dates. For the remaining cases (11/22a, 11/29a, 11/28a, 11/27a, and 11/27b), more than 59% of pixels are identified as cirrus/low cloud. All these dates were shown from weather reports to have multilayer clouds involving cirrus. The 11/26b, 11/22a, 11/29a, and 11/27b cases showed a significant presence of thick cirrus clouds. No significant presence of single-layer low clouds was observed on these dates.

Figures 5–7 show the geographical distribution of channel 4 brightness temperature [(a) frames] and the identified cloud types [(b) frames] for the three cases presented in Figs. 2–4. The cloud types identified by the detection scheme are shown in a 0.1° × 0.1° grid box. The number in each grid box represents the most prevalent cloud type within that box. The indices 0, 1, 2, 3, and 4 denote clear, cirrus, cirrus/low, thick cirrus ($T_4 < 233$ K), and low cloud, respectively. Empty grid boxes imply that data were not available. For the 6 December case, Fig. 5a shows that most of the area is clear. Near the southeastern corner, the area is shown to consist of cirrus and cirrus/low clouds (Fig. 5b). Over the northeastern corner and the center of the domain, there are two cold pockets identified as cirrus. However, the center area is counted as clear because the majority of pixels within the grid boxes involved are clear. The above distributions can be explained based on the statistics of Table 1 and the histograms shown in Fig. 2. For the majority of the pixels, $r_1 < r_{1c}$ ($=0.18$), $Q > Q_1$ ($=1.10$), BTD45 < BTD45$_{cr}$ ($=2.5$ K), and $T_4 > T_{4cr}$ ($=280$ K). Thus, they are identified as clear. The remaining pixels are identified as cloudy and are subject to further classification. For some cloudy pixels, $Q > Q_{ci1}$ ($=1.00$), while for others, $Q < Q_{ci1}$. They are identified as cirrus and cirrus/low cloud, respectively (Fig. 1). Since no pixels have BTD45 < BTD45$_{ci}$ ($=0.5$ K), no low-cloud pixels are detected. For the 5 December case, Figs. 6a,b show that almost all of the domain is covered with cirrus clouds. For the 22 November case, all of the domain is overcast as shown in Fig. 7a. The detection scheme identifies that all grid boxes except one are cirrus/low clouds. One grid box near the southeastern corner consists of cirrus alone, corresponding to the darker (warmer) area in the brightness temperature map. There are seven grid boxes of thick cirrus over the northwestern region, corresponding to the brighter (colder) area in the brightness temperature map.

TABLE 3. Percentage of the pixels identified as clear, cirrus, cirrus/low, and low cloud by the daytime clear/cloud detection scheme applied to the *NOAA-11* and *NOAA-12* HRPT pixel image over the Coffeyville area. The percentages are defined as the ratio of pixels identified in each type to the total number of pixels within the domain, multiplied by 100.

Date	Clear	Cirrus	Cirrus/low	Low
12/6b	86.7	11.5	1.8	0.0
12/5b	0.0	99.9	0.1	0.0
11/26b	0.0	84.5	15.5	0.0
11/22a	0.0	9.5	89.3	1.2
11/29a	0.0	11.5	88.2	0.3
11/28a	0.0	8.3	91.7	0.0
11/28b	1.5	85.1	13.3	0.0
11/27a	0.0	0.0	99.5	0.5
11/27b	0.0	2.5	97.5	0.0

To verify results from the cloud detection scheme, we select a 0.1° × 0.1° area around Coffeyville for each case. Based on the average wind speed at the cirrus level, the selected 0.1° × 0.1° domain of satellite data corresponds to 4 min of ground-based measurements. We compare classified cloud types with those derived from radar, lidar, and replicator measurements. From contour graphs of backscattering signals with respect to height and time, we identify the presence of clouds by the signal strength that is above certain thresholds. For the PSU radar, a height-dependent threshold was set at −60 dBZ between 0 and 1 km and at −30 dBZ above 6 km. For the ETL lidar, the minimum signal associated with clouds was set at −70 dB. This threshold eliminates the possibility of mistaking as clouds from the returning signals caused by the scattering effects of aerosols. For the LaRc lidar, the lowest limit of attenuation scattering ratio[2] associated with clouds

[2] This quantity is defined as the ratio of the measured backscattering signals to a prescribed "clear air" value.

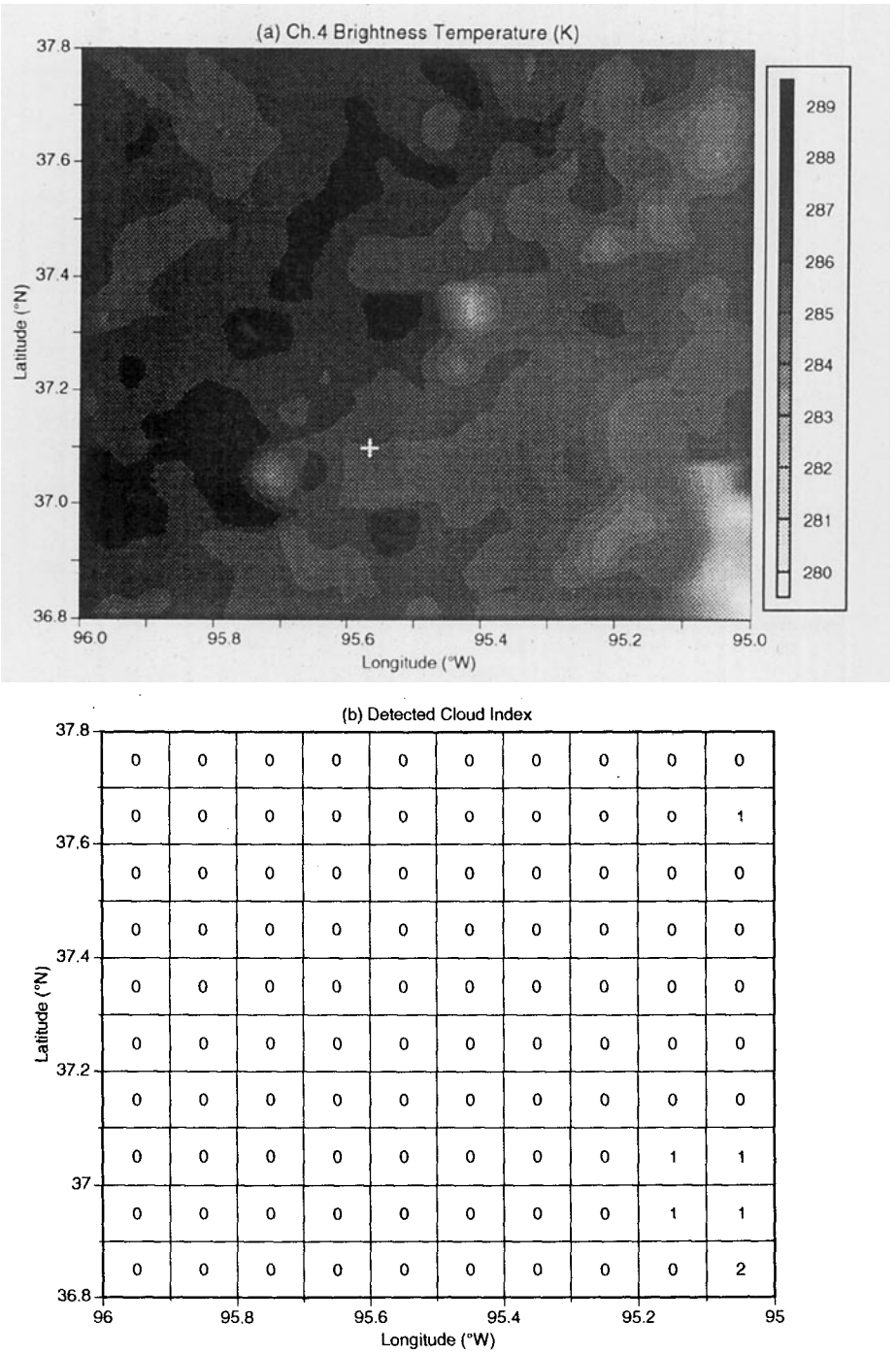

FIG. 5. (a) AVHRR channel 4 brightness temperatures over Coffeyville at 2000 UTC 6 December 1991, and (b) detected cloud types classified by number index over the same area at the same time (0—clear; 1—cirrus; 2—cirrus/low; 3—thick cirrus; 4—low).

was set at 10. Lidars tend to determine the altitude of cirrus cloud base well, but in some cases they are unable to determine the cloud-top height accurately due to occultation.

Because the replicator sonde was launched with the NCAR CLASS, we combine these measurements into one independent dataset. Cirrus clouds were present whenever the replicator sampling indicates the existence of ice crystals. We assume that the cloudy condition at the location of replicator sampling was similar as that directly over Coffeyville. This assumption appears to be valid, because in the present study cirrus

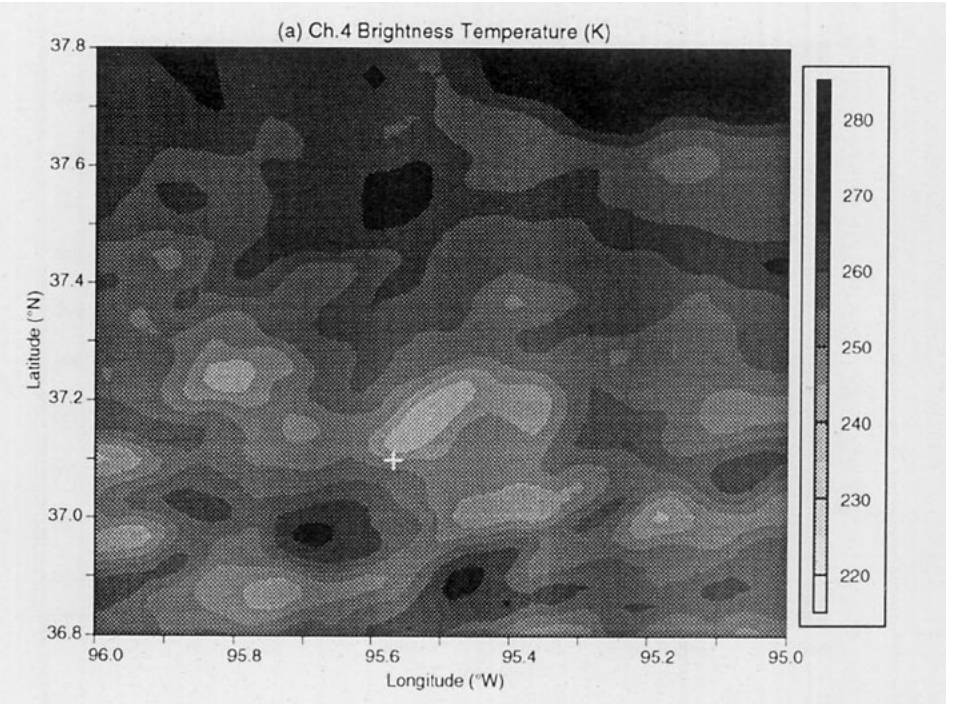

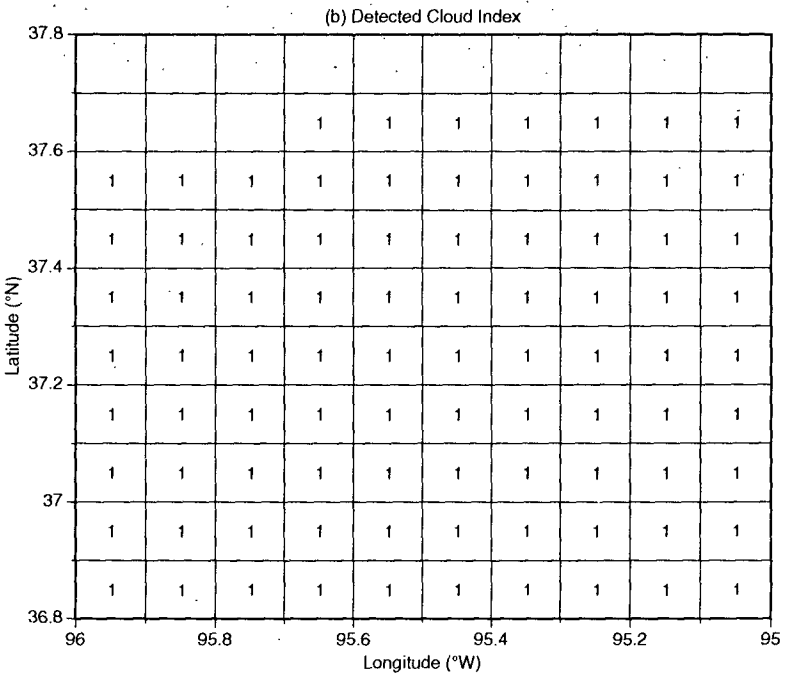

FIG. 6. Same as Fig. 5 except for the case of 2100 UTC 5 December 1991.

clouds were widespread for all cirrus and cirrus/low cases (Table 3). We also use the relative humidity profiles obtained from the NCAR CLASS as a means of identifying the presence of low clouds. Given the uncertainty of the relative humidity profile (~10%), low clouds with $T > 253$ K are present if the relative humidity is above 90%. Poore et al. (1995) use even lower temperature-dependent thresholds to determine the presence of low clouds from rawinsonde measurements. They have given a detailed discussion on the reliability of these thresholds. It is also possible to use the relationship between the ice saturation relative humidity and the temperature to identify the presence of cirrus clouds. However, as pointed out by Heymsfield

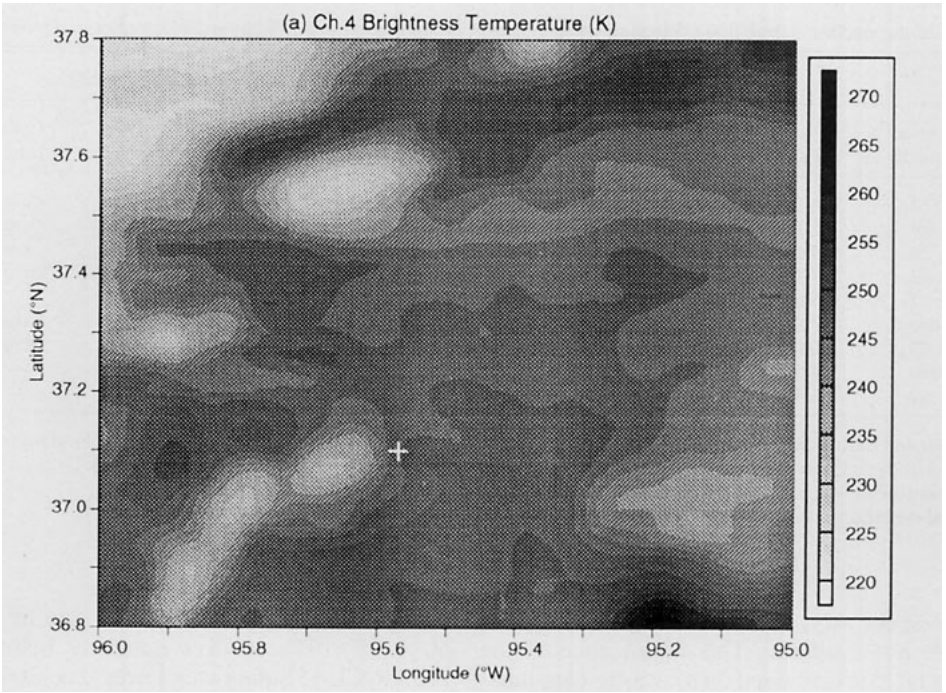

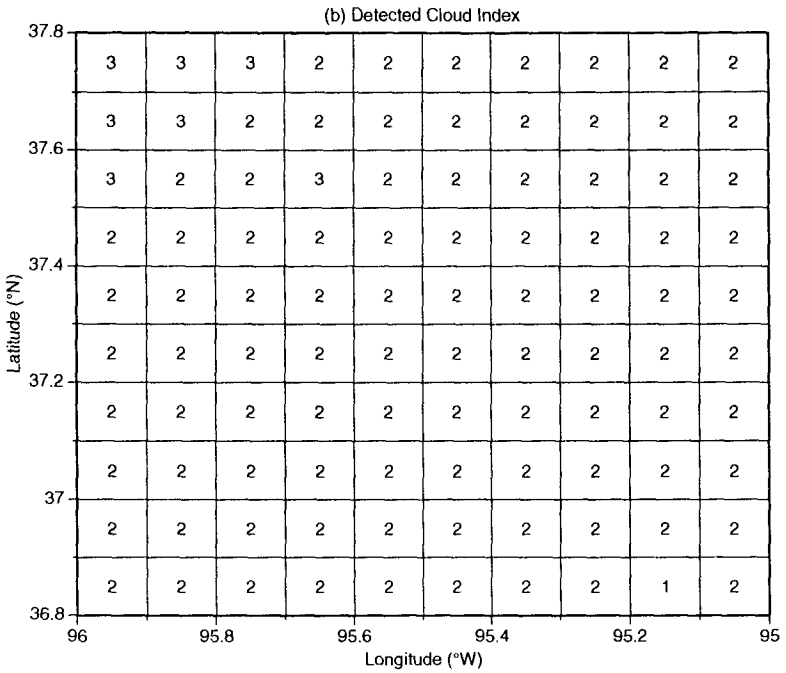

FIG. 7. Same as Fig. 5 except for the case of 1400 UTC 22 November 1991.

and Miloshevich (1993), the measurement of relative humidity by the NCAR CLASS in the upper troposphere is highly uncertain and questionable. Thus, relative humidity measurements were not used in the verification of the presence of cirrus clouds.

Table 4 summarizes the results of these verifications. Columns 3–6 list parameters determined from satellite data, while columns 7–11 give cloudy conditions obtained from satellite data and various ground-based and in situ instruments. In particular, the last column shows results from the combined replicator/NCAR CLASS measurements. The term "ice" represents the cloud particle phase registered by the replicator. The terms "low" and "dry" mean the presence and absence of

TABLE 4. Results of the satellite-based cloud detection compared with ground-based radar, lidar, and balloonborne replicator measurements.

	Parameter values					Cloudy condition				
Date	Number of pixels	r_1 (%)	Q	BTD45 (K)	T_4 (K)	Satellite	PSU radar	ETL lidar[a]	LaRc lidar[a]	Soundings
12/6b	117	12.1	1.22	0.92	287.0	clear	clear	clear	clear	—/dry
12/5b	89	32.1	1.07	3.04	249.4	cirrus	cirrus	cirrus	cirrus	ice/dry
11/26b	79	24.2	1.10	2.73	271.6	cirrus	cirrus	cirrus	cirrus	ice/dry
11/22a	93	57.7	0.91	0.46	244.7	ci/low	ci/low	cirrus	cirrus	ice/low
11/29a	52	45.6	0.89	1.18	249.7	ci/low	ci/low	—	—	ice/low
11/28a	100	23.8	0.91	2.09	272.1	ci/low	ci/low	cirrus	cirrus	ice[b]/low
11/28b	85	20.0	1.04	1.77	284.2	cirrus	cirrus	cirrus	cirrus	ice[b]/dry
11/27a[c]	5200	44.5	0.91	0.80	246.0	ci/low	ci/low	—	—	—/low
11/27b	67	63.5	0.93	3.74	262.7	ci/low	ci/low	—	—	—/low

[a] Both ETL lidar and LaRc lidar measured signals from the backscattering of boundary layer aerosols and low cloud particles. These signals were not included in the images analyzed in this study.

[b] Based on replicator measurements between the two satellite overpasses.

[c] Satellite cloud detection results are based on data over 1.0° × 1.0° area around 38.5°N, 96.5°W.

low clouds, respectively. The horizontal bar denotes that data were not available. The significance of the content of this table is discussed on a case-by-case basis in the following.

For case 12/6b, based on the average of 117 pixels, all four parameters (r_1, Q, BTD45, and T_4) pass the clear threshold tests. Thus, the pixels are classified as clear. The PSU radar, ETL lidar, and LaRc lidar backscattering measurements all showed no cloud signals near satellite overpass (2057 UTC). The weak echoes measured by the ETL lidar at 2 km were caused by tropospheric aerosols. There were no replicator measurements on that date. The NCAR CLASS relative humidity profile was less than 80%, indicating that the whole vertical column of the atmosphere was dry. Thus, all the cloud conditions obtained from the ground-based instruments and soundings are consistent. It is evident therefore that the detection of clear sky from AVHRR in this case is successful.

For case 12/5b, the selected domain was detected as consisting of cirrus, because $Q > 1.0$. ETL lidar detected cirrus clouds located between 9 and 13 km near the time of satellite overpass (2108 UTC). Major signal strength occurred at 9–10 km, which is associated with large ice crystals (mean effective size > 120 μm) undergoing partial sublimation and gravitational settling processes (Ou et al. 1995). The LaRc lidar also recorded the presence of single-layer cirrus between 9 and 12 km at the time of satellite overpass. These cloud-top heights are lower than those detected from the ETL lidar. This difference is probably due to the difference in instrument location. Note that the LaRc lidar was deployed at Parsons, about 30 km northeast of Coffeyville. During the period from 1800 to 2400 UTC, the cirrus clouds detected by the LaRc lidar were highly inhomogeneous, but the temporal variation of cloud boundaries was relatively smooth. The replicator sampled ice crystals between 9.5 and 13 km with vertically averaged mean effective size of 90 μm (Ou et al. 1995). The relative humidity below 6 km from NCAR CLASS data was lower than 70%, indicating a dry lower atmosphere. Between 9.5 and 13 km, the relative humidity varied between 50% and 30%, which was significantly lower than the corresponding ice saturation relative humidity (67%–50%). In situ aircraft (the NCAR Sabreliner) measurements recorded humidity values around ice saturation (Heymsfield and Miloshevich 1993). These differences demonstrate the uncertainty of the humidity measurements in the upper troposphere. Nevertheless, data obtained from the ground-based instruments and replicator are consistent, confirming the presence of cirrus clouds detected by satellite data.

For case 11/26b, the selected domain contains cirrus because $Q > 1.0$. The PSU radar detected the presence of cirrus clouds between 1830 and 2300 UTC with drastically varying cloud boundaries. The cloud-top height gradually dropped from 9 to 8 km. The cloud-base height showed a three-stage drop. Between 1830 and 1900 UTC, the cloud base was located at about 8 km. Between 1900 and 2100 UTC, it was at 6 km. After 2200 UTC, the cloud base dropped to 3.5 km. At satellite overpass (2111 UTC), the cloud was located between 6.1 and 8.5 km. From 2113 to 2121 UTC, the ETL lidar detected cirrus clouds between 6 and 9 km. Major echoes were located in the lower part of the cloud. The LaRc lidar also detected the presence of single-layer cirrus. Between 1800 and 2200 UTC, the cloud top lowered from 10 to 7 km, while the cloud base dropped from 8 to 5 km. At the satellite overpass, the cloud was located between 6 and 8 km. As in the ETL lidar data, the major echoes occurred near the cloud base. Occultation may have occurred for all three ground-based instruments. The replicator sampled large ice crystals between 6 and 9 km. The vertically averaged mean effective size is about 124 μm (Ou et

al. 1995). As in the case of 12/5b, the relative humidity for temperature higher than 253 K is less than 90%, indicating a dry lower atmosphere. Once again, the presence of cirrus cloud as detected by satellite data is validated by the consistent measurements of the ground-based instruments and replicator sonde.

For case 11/22a, satellite overpass was at 1445 UTC. Although the BTD45 is less than 0.5 K, the fact that $Q < 1.0$ and $T_4 < 253$ K shows the presence of cirrus/low clouds in the selected domain. Between 1300 and 1500 UTC, the PSU radar image showed an impressive presence of cirrus clouds overlying a layer of low clouds right above the ground (0–0.5 km). There were drastic variations of cloud-top and cloud-base heights between 6–8 and 4–5 km, respectively. The ETL lidar image between 1409 and 1418 UTC showed that clouds were located between 5 and 6 km. Particularly strong echoes occurred between 5 and 5.5 km. As in the ETL lidar image, the LaRc lidar image also showed strong echoes, indicating that clouds were located between 5 and 6 km during the period from 1400 to 1500 UTC. Measurements by both instruments below 1 km were discarded. For this reason, we are unable to state definitely whether low clouds were present. The relative humidity profile showed that below 0.5 km the relative humidity exceeded 90%, indicating the presence of near-ground low clouds (Fig. 8a). The presence of low clouds was also reported in the weather synopsis. Obviously, these low clouds were not sufficiently optically thick to block the lidar signals. Replicator measurements indicated the coexistence of ice crystals and water droplets, and the derived position of the upper-layer cloud (4.6–8.9 km, Fig. 8a) was consistent with lidar and radar measurements. The detection of the multilayer cloudy condition from AVHRR data agrees with ground-based observations.

For case 11/29a, satellite overpass was at 1400 UTC. The selected domain was identified as containing cirrus/low cloud, because $Q < 1.0$ and BTD45 > 0.5 K. The PSU radar image showed a significant presence of low clouds between 1330 and 1500 UTC. Based on personal communications with scientists processing the PSU radar data, we find that only echoes below 3.5 km were observed during this time period. Thus, from this image, it is not certain whether there were cirrus clouds above 3.5 km. However, replicator data collected within this time period did indicate the presence of ice crystals between 6.2 and 9.2 km. Finally, the relative humidity sounding indicated the presence of low clouds between 1 and 2 km (Fig. 8b). Both lidar measurements were not available for this date, however. Based on the combined PSU radar, replicator, and sounding measurements, it is reasonable to conclude that the cirrus/low-cloud condition was prevalent, confirming the satellite detection result.

For case 11/28a, cirrus/low clouds are shown, because $Q < 1.0$ and BTD45 > 0.5 K. The PSU radar echoes revealed the presence of sparse cirrus clouds between 8 and 11 km, as well as the presence of a low cloud between 0 and 1 km from 1330 to 1530 UTC.

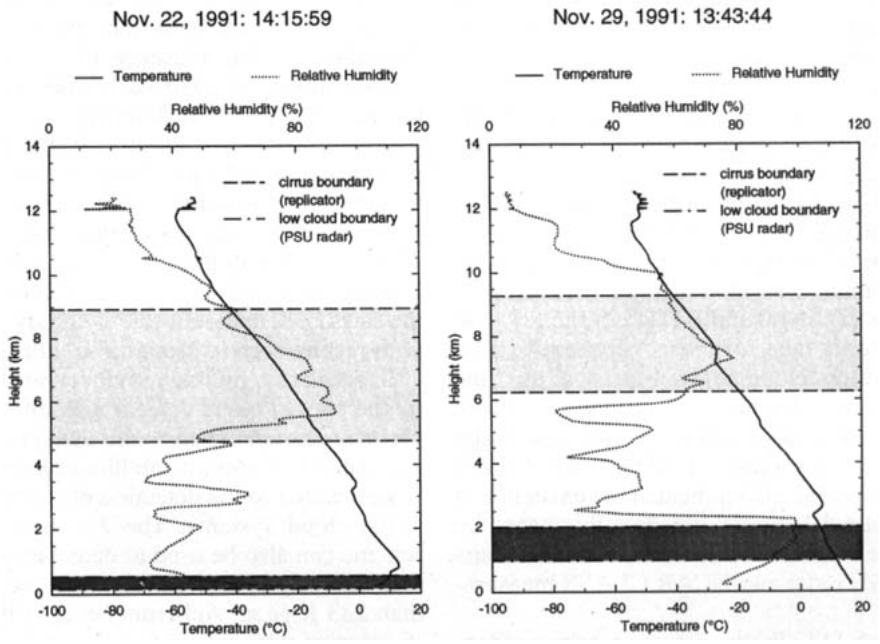

FIG. 8. Temperature and humidity profiles from NCAR CLASS soundings for (a) 1415 UTC 22 November 1991 and (b) 1343 UTC 29 November 1991. In both cases, both cirrus clouds and low clouds were present. Their positions were derived from replicator and PSU radar measurements, respectively.

The ETL lidar signals picked up cirrus between 10 and 12 km within the period from 1415 to 1425 UTC. These cirrus clouds were not detected by the PSU radar, however. The replicator data collected at 1720 UTC indicated that the ice crystals sampled within the cirrus clouds were relatively small with an average mean effective size of about 50 μm. The LaRc lidar recorded the presence of cirrus clouds between 8 and 11 km during the period from 1500 to 1600 UTC (Baum et al. 1995). The soundings showed a moist layer with the relative humidity of about 88% between 0.5 and 1.5 km. It is possible that evaporating cloud droplets could exist here. Combining measurements from all the ground-based instruments and replicator and sounding data, we conclude that the sky condition must be associated with cirrus/low clouds. This is a conclusion that can also be drawn from the satellite detection result.

For case 11/28b, the selected domain was identified from AVHRR data as consisting of cirrus clouds only ($Q > 1.0$)—a unique case. The PSU radar detected the on-and-off presence of cirrus between 8 and 10 km during the period from 1900 to 2300 UTC. The radar did not record any low clouds because signals associated with altitudes lower than 7.5 km were discarded. The ETL lidar image between 2034 and 2044 UTC showed the presence of discontinuous cirrus clouds located between 8 and 9 km. There were three broken periods caused by the blocking out of lidar signals due to the presence of thick, low clouds above 2 km. The LaRc lidar at Parsons also detected cirrus clouds at 8–11 km during the period 1900–2400 UTC. The cloud-top heights detected by the LaRc lidar were higher than those detected by the PSU radar and the ETL lidar. The inferred absence of low clouds is supported by the fact that measured relative humidity in the lower troposphere is well below saturation value. Thus, in this particular case, detection results are consistent with available measurements.

For case 11/27a, due to the limited availability of AVHRR data, the satellite cloud detection results are based on data from the 1.0° × 1.0° area around 38.5°N, 96.5°W. This domain was identified as consisting of cirrus/low clouds ($Q < 1.0$ and BTD45 > 0.5 K). The PSU radar detected a layer of cirrus between 7 and 9 km and a layer of low cloud below 1 km near the time of satellite overpass. Neither ETL lidar nor LaRc lidar images were available, and no replicator sounder was launched on that date. However, the NCAR CLASS humidity profile also indicated the existence of a layer of low cloud below 1 km. For this case, we conclude that the satellite detection results are consistent with both PSU radar and NCAR CLASS measurements.

Finally, for case 11/27b, the detection scheme identified the cirrus/low cloud condition in the selected domain, because $Q < 1.0$ and BTD45 > 0.5 K. The PSU radar image showed a distinct presence of low clouds between 1 and 2 km. The radar detected sparse presence of cirrus near the time of satellite overpass. The presence of cirrus clouds was also reported in the weather synopsis. Thus, we conclude that cirrus/low clouds were present. The satellite detection result is consistent with this conclusion.

4. Conclusions

A numerical scheme for the detection of multilayer cloud pixels involving cirrus clouds has been developed using data from AVHRR channels 1, 2, 4, and 5. The unique feature of this scheme is that it simultaneously employs the physical properties of channels 1 and 2 reflectance ratios, the brightness temperature differences between channels 4 and 5, and the channel 4 brightness temperatures to identify various cloudy conditions. In this scheme, clear pixels are first separated from cloudy pixels, which are then classified into three types: cirrus, cirrus/low cloud, and low cloud. This scheme has been applied to the satellite data collected during FIRE II IFO. Nine satellite overpasses occurring on seven observation dates have been selected, including one clear case, three single-layer cirrus cases, and five multilayer cases. Threshold values used in the detection scheme have been determined based on the statistical analyses of all the satellite data. The detection scheme has been applied to the AVHRR data on a pixel-by-pixel basis, and the results mapped on a 1° × 1° area surrounding the key observational site.

To validate the detection results, we have obtained ground-based lidar and radar time–height images as well as replicator and NCAR CLASS sounding data. We have analyzed these data on a case-by-case basis and identified the presence of clouds using the prescribed thresholds. For each case, we have discussed the reasons for the differences in cloud detection by various instruments. In general, the presence/absence of clouds inferred from different instruments is consistent and complementary. We have compared the satellite-detected cloudy conditions based on a 0.1° × 0.1° area average with those inferred from the independent ground-based and in situ measurements. In every case, the satellite detection result of cloudy conditions agrees with results derived from those independent data.

In summary, multilayer clouds are clearly identified by the present cloud detection scheme, as supported by verifications against the combined ground-based and in situ data. The present satellite remote sensing scheme is well suited to the detection of midlatitude multilayer cirrus cloud systems. The T_{4c1} threshold test in this scheme can also be used to detect tropical anvils, since their IR brightness temperatures are typically colder than 233 K (e.g., Ackerman et al. 1988). Further verification of this scheme for other time periods and geographical locations depends on the availability of in situ and ground-based measurements of future field campaigns.

Acknowledgments. This research was supported by NASA Grants NAG5-1050 and NAG1-1719 and Air Force Geophysics Directorate Contract F19628-95-K-002. We thank E. Clothiaux and Tom Ackerman for making available PSU radar images, J. Intrieri and W. Eberhard for supplying ETL lidar images, J. Alvarez for providing LaRc lidar images, and A. Heymsfield for cloud replicator data. Helpful discussions with E. Clothiaux and J. Intrieri are appreciated. We are also grateful to two anonymous reviewers for their detailed and constructive comments. Information on FIRE data summary has been provided by Dr. K. Sassen.

REFERENCES

Ackerman, T. P., K. N. Liou, F. P. J. Valero, and L. Pfister, 1988: Heating rates in tropical anvils. *J. Atmos. Sci.*, **45,** 1606–1623.

Alvarez, J. M., 1994: *LaRc Lidar Data User's Guide.* [Available on-line at Langley DAAC User Service:telnet: //eosdis.larc.nasa.gov.]

Arking, A., and J. D. Childs, 1985: Retrieval of cloud cover parameters from multispectral satellite images. *J. Climate Appl. Meteor.*, **24,** 322–333.

Baum, B. A., R. F. Arduini, B. A. Wielicki, P. Minnis, and S. C. Tsay, 1994: Multilevel cloud retrieval using multispectral HIRS and AVHRR data: Nighttime oceanic analysis. *J. Geophys. Res.*, **99,** 5499–5514.

——, and Coauthors, 1995: Satellite remote sensing of multiple cloud layers. *J. Atmos. Sci.*, **52,** 4210–4230.

Chou, M. D., J. Childs, and P. Dorian, 1986: Cloud cover estimation using bispectral satellite measurements. *J. Climate Appl. Meteor.*, **25,** 1280–1292.

Clothiaux, E. E., M. A. Miller, B. A. Albrecht, T. P. Ackerman, J. Verlinde, D. M. Babb, R. M. Peters, and W. J. Syrett, 1995: An evaluation of a 94-GHz radar for remote sensing of cloud properties. *J. Atmos. Oceanic Technol.*, **12,** 201–229.

d'Entremont, R. P., 1986: Low and midlevel cloud analysis using nighttime multispectral imagery. *J. Climate Appl. Meteor.*, **25,** 1853–1869.

Hahn, C. J., S. G. Warren, J. London, R. M. Chervin, and R. Jenne, 1982: Atlas of simultaneous occurrence of different cloud types over the ocean. NCAR Tech. Note TN-201+STR, 212 pp.

——, ——, ——, ——, and ——, 1984: Atlas of simultaneous occurrence of different cloud types over land. NCAR Tech. Note TN-241+STR, 216 pp.

Heymsfield, A. J., and L. M. Miloshevich, 1993: Overview of microphysics and state parameter measurements from FIRE-II. FIRE cirrus results, *Proc. FIRE Cirrus Science Conf.*, Breckenridge, CO, 1–4.

Inoue, T., 1987: A cloud type classification with NOAA 7 split-window measurements. *J. Geophys. Res.*, **92,** 3991–400.

Kidwell, K. B., 1991: *NOAA Polar Orbiter Data Users' Guide.* 280 pp. [Available from NOAA-NCDC-SDSD, Information Processing Division, Federal Office Building #3, Room G-233, Washington, DC 20233.]

Liou, K. N., 1986: Influence of cirrus clouds on weather and climate processes: A global perspective. *Mon. Wea. Rev.*, **114,** 1167–1199.

——, 1992: *Radiation and Cloudy Processes in the Atmosphere: Theory, Observation, and Modeling.* Oxford University Press, 487 pp.

Matveev, L. T., 1984: *Cloud Dynamics.* D. Reidel, 340 pp.

Minnis, P., and E. F. Harrison, 1984: Diurnal variability of regional cloud and clear-sky radiative parameters derived from GOES data. Part I: Analysis method. *J. Climate Appl. Meteor.*, **23,** 993–1011.

——, D. F. Young, K. Sassen, J. M. Alvarez, and C. J. Grund, 1990: The 27–28 October 1986 FIRE IFO cirrus case study: Cirrus parameter relationships derived from satellite and lidar data. *Mon. Wea. Rev.*, **118,** 2402–2425.

Ou, S. C., K. N. Liou, W. M. Gooch, and Y. Takano, 1993: Remote sensing of cirrus cloud parameters using advanced very-high resolution radiometer 3.7 and 10.9 μm channels. *Appl. Opt.*, **32,** 2171–2180.

——, and Coauthors, 1995: Remote sounding of cirrus cloud optical depths and ice crystal sizes from AVHRR data: Verification using FIRE II IFO measurements. *J. Atmos. Sci.*, **52,** 4143–4158.

Poore, K. D., J. Wang, and W. B. Rossow, 1995: Cloud layer thicknesses from a combination of surface and upper-air observations. *J. Climate,* **8,** 550–568.

Post, M. J., and R. E. Cupp, 1990: Optimizing a pulsed Doppler lidar. *Appl. Opt.*, **29,** 4145–4158.

Rao, N. X., S. C. Ou, and K. N. Liou, 1995: Removal of the solar component in AVHRR 3.7-μm radiances for the retrieval of cirrus cloud parameters. *J. Appl. Meteor.*, **34,** 482–499.

Rogers, R. R., and M. K. Yau, 1989: *A Short Course in Cloud Physics.* 3d ed. Pergamon Press, 293 pp.

Rossow, W. B., and A. A. Lacis, 1990: Global, seasonal cloud variation from satellite radiance measurements. Part II: Cloud properties and radiative effects. *J. Climate,* **3,** 1204–1253.

Saunders, R. W., and K. T. Kriebel, 1988: An improved method for detecting clear sky and cloudy radiances from AVHRR data. *Int. J. Remote Sens.*, **9,** 123–150.

Tian, L., and J. A. Curry, 1989: Cloud overlap statistics. *J. Geophys. Res.*, **94,** 9925–9935.

Uttal, T., and J. M. Intrieri, 1993: Comparison of cloud boundaries measured with 8.6 mm radar and 10.6 μm lidar. *Proc. of the Topical Symp. on Combined Optical–Microwave Earth and Atmospheric Sensing,* Albuquerque, NM, IEEE Geoscience and Remote Sensing Society, 207–210.

Weinreb, M. P., G. Hamilton, and S. Brown, 1990: Nonlinearity corrections in calibration of advanced very high resolution radiometer infrared channels. *J. Geophys. Res.*, **95,** 7381–7388.

Whitlock, C. H., S. R. LeCroy, and R. J. Wheeler, 1994: SRB/FIRE satellite calibration results and their impact on ISCCP. *Proc. Eighth Conf. on Atmospheric Radiation,* Nashville, TN, Amer. Meteor. Soc., 52–54.